NUCLEI
Experiment

Photoneutron Reactions in Astrophysics

V. V. Varlamov[1]*, B. S. Ishkhanov[1],[2], V. N. Orlin[1], N. N. Peskov[1], and K. A. Stopani[1]

Received January 13, 2014; in final form, May 19, 2014

Abstract—Among key problems in nuclear astrophysics, that of obtaining deeper insight into the mechanism of synthesis of chemical elements is of paramount importance. The majority of heavy elements existing in nature are produced in stars via radiative neutron capture in so-called s- and r processes, which are, respectively, slow and fast, in relation to competing β^--decay processes. At the same time, we know 35 neutron-deficient so-called bypassed p-nuclei that lie between ^{74}Se and ^{196}Hg and which cannot originate from the aforementioned s- and r-processes. Their production is possible in $(\gamma, n), (\gamma, p)$, or (γ, α) photonuclear reactions. In view of this, data on photoneutron reactions play an important role in predicting and describing processes leading to the production of p-nuclei. Interest in determining cross sections for photoneutron reactions in the threshold energy region, which is of particular importance for astrophysics, has grown substantially in recent years. The use of modern sources of quasimonoenergetic photons obtained in processes of inverse Compton laser-radiation scattering on relativistic electrons makes it possible to reveal rather interesting special features of respective cross sections, manifestations of pygmy $E1$ and $M1$ resonances, or the production of nuclei in isomeric states, on one hand, and to revisit the problem of systematic discrepancies between data on reaction cross sections from experiments of different types, on the other hand. Data obtained on the basis of our new experimental–theoretical approach to evaluating cross sections for partial photoneutron reactions are invoked in considering these problems.

1. INTRODUCTION

A determination of the mechanisms of chemical-element production is one of the fundamental problems in modern natural sciences, which lies on the border of nuclear physics and astrophysics. Important information about the nature of elements is contained in the well-known A dependence of their abundances. The abundance in question decreases fast as the mass number increases, and the whole A dependence admits a clear-cut partition into two regions: that of relatively light and medium-mass elements, $A < 70$, and that of heavy elements, $A \sim 70$–200 [1].

In the region of $A < 70$, nuclei are produced in the following processes: hydrogen burning, which leads to the formation of nuclei of up to helium; helium burning, which leads to the formation of carbon, oxygen, and neon nuclei; alpha-particle-capture processes leading to the formation of nuclei of up to calcium; and the e-process, which leads to the formation of the iron-peak nuclei. The so-called X-process in which lithium, beryllium, and boron isotopes are produced via the spallation of heavier isotopes under the

effect of cosmic-ray particles can also be associated with this region of nuclei ($A < 70$).

Processes of radiative neutron capture proceed in the region of $A \sim 70$–200. These are so-called s- and r-processes, which are, respectively, slow and fast in relation to competing β^--decay processes. In the slow s-process, β^--decay rate is higher than the neutron-capture rate. The formation of new comparatively stable nuclei proceeds via a successive addition of neutrons, involving only stable and β^--radioactive nuclei with long half-lives along the β^--stability value. In the fast r-process, many heavy nuclei are produced via a fast sequential capture of a large number of neutrons. When the capture rate becomes lower than the β^--decay rate, the nucleus produced under these conditions decays, and sequential neutron capture begins anew. The line along which nuclei are produced in the r-process is shifted with respect to the stability path (track of the s-process) toward neutron-rich isotopes.

In the region of heavy elements, maxima in the mass-number regions of $A \sim 80$–98, 130–138, and 195–208 are quite distinct. These maxima correlate with the neutron-magic numbers of $N = 50$, 82, and 126 and manifest themselves in the s-process. Similar maxima at smaller mass numbers (in the ranges

[1] Skobeltsyn Institute of Nuclear Physics, Moscow State University, Moscow, 119991 Russia.
[2] Faculty of Physics, Moscow State University, Moscow, 119991 Russia.
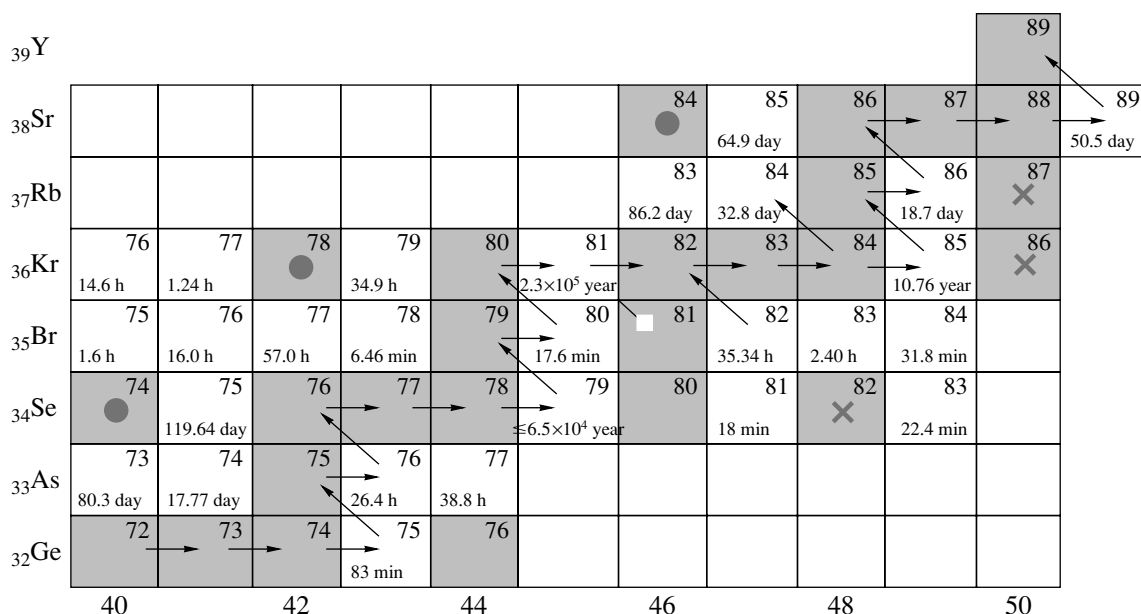*E-mail: Varlamov@depni.sinp.msu.ru

Fig. 1. Diagram (the number of neutrons, N, and the number of protons, Z, are plotted along the abscissa and ordinate, respectively) illustrating the relative contributions of s-, r-, and p-processes in the region of $72 \leqslant A \leqslant 89$. The gray and white boxes contain, respectively, stable and unstable isotopes (the mass numbers A and the lifetimes are presented). The arrows indicate a typical motion for the s-process; the crosses mark the isotopes ($^{82}_{34}$Se, $^{86}_{36}$Kr, and $^{87}_{37}$Rb) produced in the r-process; and the circles show isotopes ($^{74}_{34}$Se, $^{78}_{36}$Kr, and $^{84}_{38}$Sr) whose production is possible only in the p-process.

of 78−84, 126−132, and 189−197, respectively) are associated with the r-process [2].

In this region, so-called p-processes leading to the production of a large number of heavy elements that have neutron-deficient nuclei from the beta-stability valley are possible in addition to s- and r-processes, which cannot produce these elements. For 35 known nuclei of this group (see Table 1; see also [3−5]) from Se ($Z = 34$) to Hg ($Z = 80$), which are referred to as bypassed ones, to arise, it is necessary to invoke mechanisms other than radiative neutron capture and β^- decay. A typical diagram of the s-, r-, and p-processes in the region of $72 \leqslant A \leqslant 89$ is given in Fig. 1.

It can clearly be seen that the bypassed nuclei cannot be obtained on the trajectories of s and r processes, which are characterized by motion from the left to the right with the addition of neutrons. For their emergence, one needs inverted motion, from the right to the left, accompanied by neutron knockout. This direction of motion over the diagram of elements can be explained [2] by various mechanisms: (p, n) charge-exchange reactions, (p, γ) proton-capture reactions, weak interaction in positron capture, spallation under the effect of protons and alpha particles accelerated in supernova envelopes, and reactions involving intense neutrino fluxes from supernova explosions, but, first of all, (γ, n) and $(\gamma, 2n)$ photonuclear reactions.

Various processes, including the annihilation of particles and antiparticles produced upon the Big Bang, bremsstrahlung from electrons and positrons, the inverse Compton scattering of photons on high-energy electrons, neutral-pion decay to two photons, gamma transitions between excited states of nuclei, electron acceleration in an inhomogeneous interstellar plasma, and gamma radiation from supernovae and actives galaxy cores may be sources of photons in stars and cosmic space with energies that are sufficient for initiating photonuclear reactions. The energies of photons from such processes are distributed over a very wide region extending from 10^{-1} to 10^7 keV. Starting from several MeV units, this energy is sufficient for ensuring the photodisintegration of nuclei.

Although the abundances of elements produced in p-processes are two to three orders of magnitude less than the abundances of elements produced in s- and r-processes, the role of p-processes—first of all, photoneutron reactions—is very important, since, without them, it is impossible to explain the origin of considerable number of elements.

2. EXPERIMENTAL INVESTIGATION OF PHOTONEUTRON REACTIONS

A large number of laboratory experiments devoted primarily to determining cross sections for processes
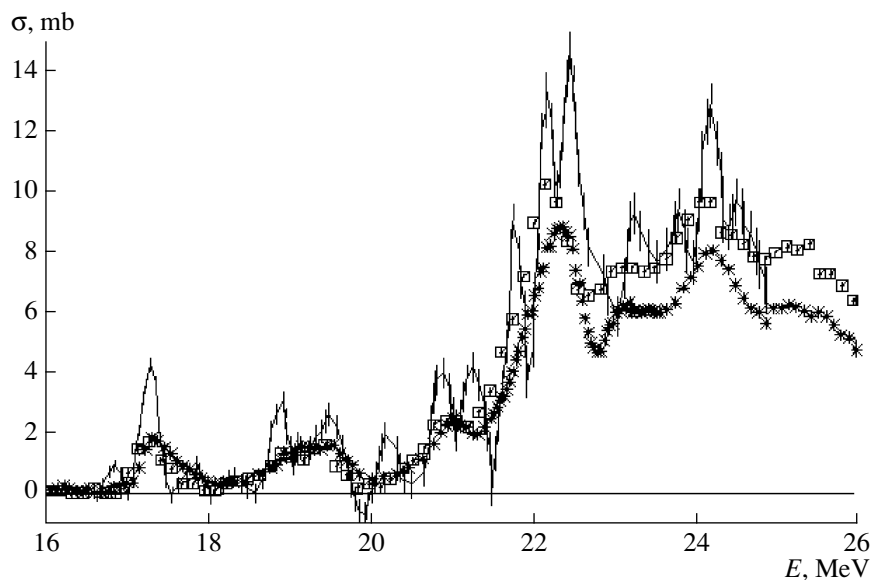
Fig. 2. Comparison of data on the cross section for the reaction $^{16}O(\gamma, n)$ that were obtained in experiments with bremsstrahlung gamma radiation (points with error bars) at the Skobeltsyn Institute of Nuclear Physics (Russia) [12] and with quasimonochromatic photons from electron−positron annihilation in Saclay (France) [13] (open boxes) and at the Lawrence Livermore National Laboratory (USA) [14] (asterisks).

involving the production of various numbers of neutrons have been performed to date with the aim of obtaining systematic data on photonuclear reactions in which final-state nuclei are produced not only in the ground states but also in isomeric states.

Experimental investigation of photonuclear reactions is complicated by a number of their special features. The absence of intense beams of monoenergetic photons is the most important of them. Such photons can be obtained by using radioactive nuclei or reactions of radiative neutron capture, but, in either case, only a limited set of discrete gamma lines having a moderately low intensity are available. The method of obtaining monoenergetic tagged photons of bremsstrahlung generated by electrons was used to determine only several reaction cross sections because of serious experimental difficulties (detection of photons that are being identified in coincidence with scattered electrons) and because of a low intensity.

For this reason, experimentalists have to apply various methods for obtaining quite intense sources of quasimonoenergetic photons that can be interpreted as photons close to monoenergetic ones. Among these, two became the most popular. The first employs bremsstrahlung photons along with special data-processing methods [6]. The second uses the radiation from relativistic positrons undergoing in-flight annihilation and the difference procedure for removing bremsstrahlung from them [7].

In recent years, quasimonoenergetic-photon beams formed upon the inverse Compton scattering of photons from a powerful laser on a beam

of high-energy electrons have ever become more widespread [8].

Many experimental data on cross sections for both total and partial photonuclear reactions involving the emission of various numbers of neutrons, protons, and other particles, as well as ions, were obtained with the aid of the first two methods. These experimental data are presented in many review articles (for example, [7]), atlases (for example, [9, 10]), and databases (for example, [11]) and are widely used both in fundamental investigations and in various applications.

Since the conditions under which information about the reaction cross sections was obtained in the aforementioned experiments were different, there were substantial discrepancies between their results. One can see this from Fig. 2, which gives data on the cross section for the neutron yield on ^{16}O nuclei,

$$\sigma(\gamma, xn) = \sigma[(\gamma, 1n) + 2(\gamma, 2n) \qquad (1)$$
$$+ 3(\gamma, 3n) + \ldots],$$

from an experiment with bremsstrahlung gamma radiation [12] and from two experiments with quasimonoenergetic photons from the annihilation process [13, 14]. Since the energy threshold for the reaction $^{16}O(\gamma, 2n)^{14}O$ is $B2n = 28.9$ MeV, Fig. 2 actually gives data on the cross section for the reaction $^{16}O(\gamma, 1n)^{15}O$.

Table 1. List of isotopes classed as p-nuclides [3] (data on abundances are presented in units in which the abundance of silicon is 10^6)

Nucleus	Abundance	Error, %	Abundance	Error, %
	[4]		[5]	
^{74}Se	0.55	6.4	0.6	5.0
^{78}Kr	0.153	18.0	0.19	
^{84}Sr	0.132	8.1	0.12	5.0
^{92}Mo	0.378	5.5	0.38	5.0
^{94}Mo	0.236	5.5	0.23	5.0
^{96}Ru	0.103	5.4	0.1	10.0
^{98}Ru	0.035	5.4	0.03	10.0
^{102}Pd	0.0142	6.6	0.014	10.0
^{106}Cd	0.0201	6.5	0.02	10.0
^{108}Cd	0.0143	6.5	0.014	10.0
^{113}In	0.0079	6.4	0.008	10.0
^{112}Sn	0.0372	9.4	0.036	10.0
^{114}Sn	0.0252	9.4	0.024	10.0
^{115}Sn	0.0129	9.4	0.013	10.0
^{120}Te	0.0043	10.0	0.0045	10.0
^{124}Xe	0.00571	20.0	0.005	
^{126}Xe	0.00509	20.0	0.004	
^{130}Ba	0.00476	6.3	0.005	5.0
^{132}Ba	0.00453	6.3	0.005	5.0
^{138}La	0.000409	2.0	0.0004	5.0
^{136}Ce	0.00216	1.7	0.002	5.0
^{138}Ce	0.00284	1.7	0.003	5.0
^{144}Sm	0.008	1.3	0.008	5.0
^{152}Gd	0.00066	1.4	0.001	5.0
^{156}Dy	0.000221	1.4	0.0002	5.0
^{158}Dy	0.000378	1.4	0.0004	5.0
^{162}Er	0.000351	1.3	0.0004	5.0
^{164}Er	0.00404	1.3	0.0042	5.0
^{168}Yb	0.000322	1.6	0.0003	5.0
^{174}Hf	0.000249	1.9	0.0003	5.0
^{180}Ta	2.48e-06	1.8	2.00e-06	10.0
^{180}W	0.000173	5.1	0.0002	7.0
^{184}Os	0.000122	6.3	0.0001	5
^{190}Pt	0.00017	7.4	0.0001	10.0
^{196}Hg	0.00048	12.0	0.001	20.0

3. DISCREPANCIES BETWEEN THE RESULTS OF DIFFERENT EXPERIMENTS

The results of the experiment with bremsstrahlung photons [12] and the experiments with annihilation photons [13, 14] in Fig. 2 differ substantially in shape—basic structural features manifesting themselves clearly in [12] show only vague signatures of their presence in [13, 14]. Dedicated investigations (see, for example, [15, 16]) revealed that these discrepancies in the structure of the reaction cross sections are due to the difference in the attained energy resolution ΔE. In experiments with bremsstrahlung photons, this resolution proves to be close to the value declared on the basis of the width of the respective line in the matrix of the inverse problem (1) (in the specific case being considered, $\Delta E = 200$ keV), but, in the annihilation experiments, ΔE is several times poorer than the values declared (in the specific cases being considered, $\Delta E = 180-280$ and $200-300$ keV, respectively) on the basis of data on the width of the annihilation line in the spectrum of radiation from positrons. The poorer resolution is due to the effect of bremsstrahlung in the photon spectrum; the difference procedure used is unable to remove this effect completely. The data from [12] and [13] agree well in magnitude (the cross section from [13] is as if a smoothed version of the cross section from [12]). This is confirmed by the relative proximity of the integrated cross sections—36.9 and 34.6 MeV mb, respectively. At the same time, the cross section from [14] proves to be substantially smaller (the integrated cross section is 28.6 MeV mb).

The errors that could be made in the Livermore experiment [14] in determining the photon flux and/or the neutron-detector efficiency were indicated in [17] as the possible reasons behind the discrepancies between the aforementioned data in magnitude. On the basis of an analysis of more than 500 cross sections for the neutron-yield reaction in (1) on nuclei from ^{2}H to ^{238}U, it was found in [18, 19] that the integrated cross sections obtained in the Livermore experiments are smaller in magnitude by $R = 6-16\%$ (the mean ratio of the integrated cross sections is $\langle R \rangle = 1.12 \pm 0.24$) than the data from the other experiments. The inclusion of the correction $\langle R \rangle$ in the data from [14] leads to an integrated-cross-section value of $28.6 \times 1.12 = 32.0$ MeV mb—that is, this shifts those data toward the data presented in [12, 13].

In the foregoing, we have considered an example of the discrepancy between the data obtained by detecting all neutrons produced in the reaction in the photon-energy region where the reaction involving the production of two neutrons is energetically impossible. In the region of energies exceeding the
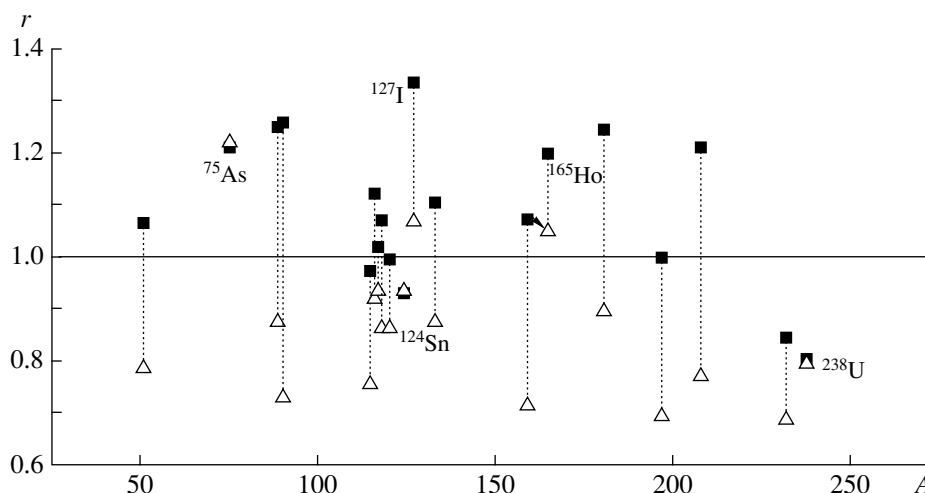
Fig. 3. Systematics of ratios of integrated cross sections, $r = \sigma_{\text{Saclay}}^{\text{int}}/\sigma_{\text{Livermore}}^{\text{int}}$, according to data on the cross sections (closed boxes) $\sigma(\gamma, 1n)$ and (open triangles) $\sigma(\gamma, 2n)$.

$(\gamma, 2n)$ threshold $B2n$, the discrepancies in magnitude between the results of the different experiments devoted to determining cross sections for $(\gamma, 1n)$ and $(\gamma, 2n)$ partial photoneutron reactions reach about 60 to 100%. Data on these reactions were predominantly obtained in beams of quasimonoenergetic photons from the annihilation process in the Saclay and Livermore experiments. The detailed comparison in [20] of the cross sections $\sigma(\gamma, 1n)$ and $\sigma(\gamma, 2n)$ obtained in the two laboratories in question for 19 nuclei (^{51}V, ^{75}As, ^{89}Y, ^{90}Zr, ^{115}In, ^{116,117,118,120,124}Sn, ^{127}I, ^{133}Cs, ^{159}Tb, ^{165}Ho, ^{181}Ta, ^{197}Au, ^{208}Pb, ^{232}Th, and ^{238}U) revealed that these discrepancies have a pronouncedly systematic character. As a rule, the cross sections $\sigma(\gamma, 1n)$ are larger in the Saclay experiment, while the cross sections $\sigma(\gamma, 2n)$ are larger in the Livermore experiment. One can clearly see this from Fig. 3, which, for all 19 nuclei mentioned above, gives the ratios $r = \sigma_{\text{Saclaofy}}^{\text{int}}/\sigma_{\text{Livermore}}^{\text{int}}$ of the integrated cross sections $\sigma(\gamma, 1n)$ and $\sigma(\gamma, 2n)$ for the reactions studied in the Saclay and Livermore experiments.

The investigations of the discrepancies in [21–24] revealed that they stem from the flaws in the method used in both laboratories for photoneutron-multiplicity sorting on the basis of experimentally measuring the kinetic energies of neutrons. This method relies on the assumption that both neutrons from a $(\gamma, 2n)$ reaction must have kinetic energies lower than the energy of the neutron from the respective $(\gamma, 1n)$ reaction, in which case one perform the necessary separation of reactions. In [25], it was shown that an increase in the photon energy and the opening of the possibility for the emission of two neutrons do not change strongly a general shape of

the neutron spectrum. In [24], it was found that, upon the photodisintegration of a ^{181}Ta nucleus at the photon energy of 25 MeV, the first neutron from the respective $(\gamma, 2n)$ reaction has a mean energy of about 4 MeV, while the second one has a mean energy of about 1.4 MeV. In the case of a similar relationship between the energies of the first and second neutrons from the respective $(\gamma, 3n)$ reaction, the energy of the second neutron from this reaction is substantially higher than the energy of the third neutron.

4. NEW APPROACH TO EVALUATING CROSS SECTIONS FOR PARTIAL PHOTONEUTRON REACTIONS

The foregoing indicates that the reliability of data obtained for the cross sections for partial photoneutron reactions with the aid of the method of neutron-multiplicity sorting calls for improvement. For this purpose, criteria of reliability of data on the cross sections for (γ, in) partial photoneutron reactions were proposed in [20, 23] in the form of transition multiplicity functions, which are ratios of cross sections for specific partial reactions to the cross section for the neutron yield; that is,

$$F_i = \sigma(\gamma, in)/\sigma(\gamma, xn) = \sigma(\gamma, in)/[\sigma(\gamma, 1n) \quad (2)$$
$$+ 2\sigma(\gamma, 2n) + \ldots + 3\sigma(\gamma, 3n) + \ldots].$$

For $i = 1, 2, 3, \ldots$, the functions F_i should not have values in excess of, respectively, 1.00, 0.50, 0.33, ... If, in some photon-energy regions, the functions F_i exceed these limiting values, this is indicative of an incorrect neutron distribution among partial reactions. The function F_2, which makes it possible to get an idea of the reliability of data on three reactions [$\sigma(\gamma, 1n)$, $\sigma(\gamma, 2n)$, and $\sigma(\gamma, 3n)$] simultaneously, is
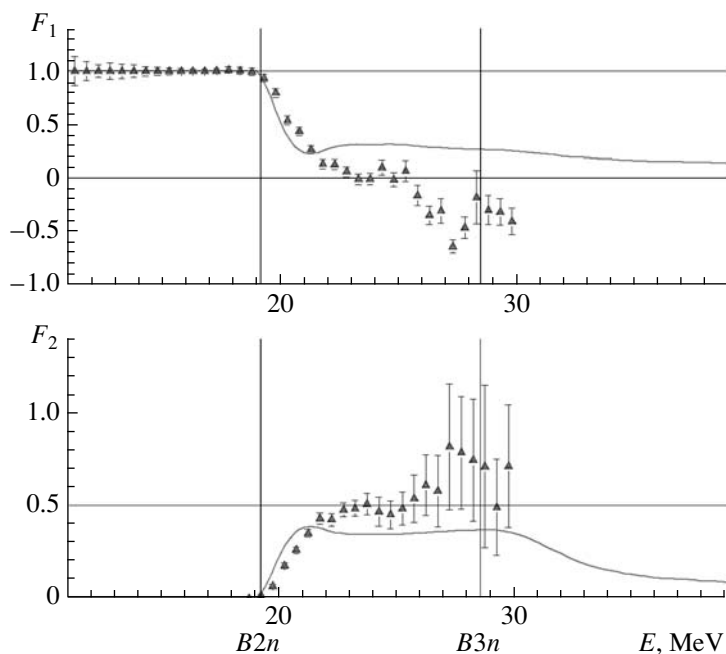
Fig. 4. Energy dependence of the functions $F_{1,2}$ obtained in [24] on the basis of experimental data from [26] ($F_{1,2}^{\text{expt}}$ represented by triangles) and the results of theoretical calculations from [27, 28] ($F_{1,2}^{\text{theor}}$ represented by curves) for the ^{91}Zr nucleus.

the most interesting and the most informative. If the function F_2 exceeds the absolute limit of 0.50 in the energy region extending to $B3n$ from below, this means a physically incorrect determination of $\sigma(\gamma, 2n)$ and, hence, of $\sigma(\gamma, 1n)$, but, if this occurs energies above $B3n$, the determination of $\sigma(\gamma, 2n)$ and $\sigma(\gamma, 3n)$ is physically incorrect.

The systematic investigations performed in [21–24] revealed that, for a large number of nuclei (^{91,94}Zr, ^{115}In, ^{112,114,116,117,118,119,120,122,124}Sn, ^{159}Tb, ^{181}Ta, ^{188,189,190,192}Os, and ^{208}Pb), there are regions of unreliable data in the energy dependences obtained for the functions $F_{1,2,3}^{\text{expt}}$ from experimental data. Figure 4 shows quite a typical example of the energy dependences obtained in [24] for the functions $F_{1,2}$ on the basis of experimental data for the ^{91}Zr nucleus [26]. One can clearly see that, in the energy region of $E > 24$ MeV, the ratio of experimental cross sections $\sigma(\gamma, 1n)$ and $\sigma(\gamma, 2n)$ is unreliable, since F_2^{expt} lies in the region of physically forbidden values in excess of 0.50, while F_1^{expt} lies in the region of physically forbidden negative values. Figure 4 also presents the functions $F_{1,2}^{\text{theor}}$ obtained in [24] on the basis of data calculated within the combined model of photonuclear reactions that was proposed in [27, 28]. They give an idea of the energy dependence of such functions whose determination is not plagued by

problems arising upon the application of the experimental method of neutron-multiplicity sorting.

The calculations based on the model developed in [27, 28] lead to good agreement with experimental data on the neutron-production cross sections $\sigma(\gamma, xn)$ (1) for medium-mass and heavy nuclei; the distinctions between the results of the different experiments for these cross sections do not exceed 12% and have nothing to do with problems of neutron-multiplicity sorting. In this connection, a method for evaluating cross sections for partial photoneutron reactions was proposed in [21, 22, 29]. This method is based on simultaneously employing the experimental neutron-production cross section $\sigma^{\text{expt}}(\gamma, xn)$ and the functions $F_{1,2,3}^{\text{theor}}$ calculated within the aforementioned model; that is,

$$\sigma^{\text{eval}}(\gamma, in) = F_i^{\text{theor}} \sigma^{\text{expt}}(\gamma, xn). \qquad (3)$$

Figure 5 gives an example of the distinctions between the evaluated and experimental cross sections for the reactions ^{91}Zr$(\gamma, 1n)^{90}$Zr and ^{91}Zr$(\gamma, 2n)^{89}$Zr, while Fig. 6 provides similar information about the reaction ^{118}Sn$(\gamma, 1n)^{117}$Sn. It is noteworthy that the cross sections evaluated in [21] are at odds with data obtained via neutron-multiplicity sorting in [30, 31], but that they agree with data obtained with the aid of inverse Compton scattering of electrons on laser radiation—a new source of quasimonoenergetic photons [8].
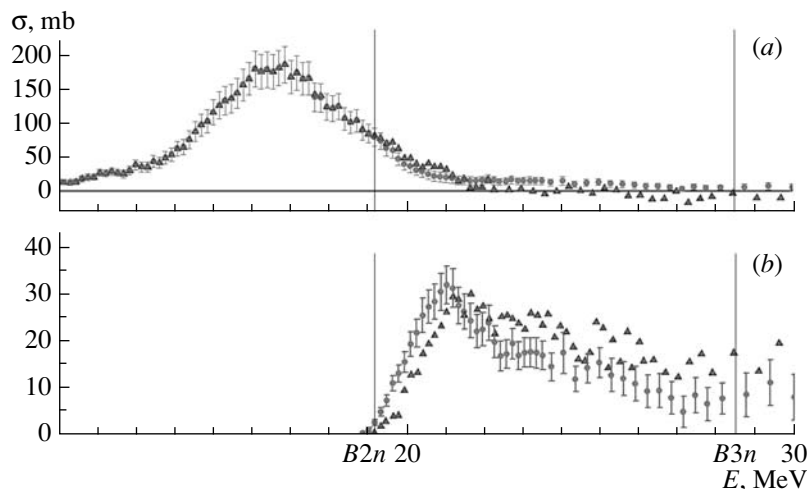
Fig. 5. Comparison of evaluated [24] (closed circles with error bars) and experimental [26] (closed triangles) reaction cross sections for the ^{91}Zr nucleus: (a) $\sigma(\gamma, 1n)$ and (b) $\sigma(\gamma, 2n)$.

5. ROLE OF PHOTONEUTRON REACTIONS IN THE PRODUCTION OF ELEMENTS

In the foregoing, we have mentioned the presence in nature of 35 bypassed elements from Se ($Z = 34$) to Hg ($Z = 80$). These elements cannot originate from s- and r-processes, so that resort to p-processes is necessary in order to explain their existence. Photoneutron reactions play the most important role among p-processes.
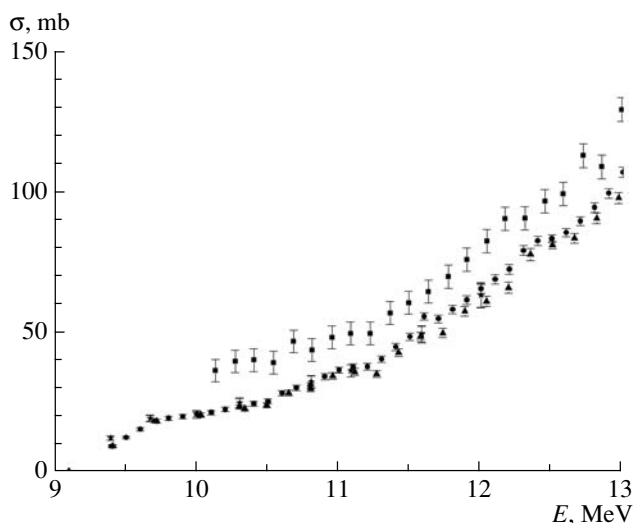
Fig. 6. Evaluated cross sections for the reaction ^{118}Sn$(\gamma, 1n)^{117}$Sn in the vicinity of the threshold from [21] (closed circles) and with their experimental counterparts from [29] (open boxes), [31] (closed triangles), and [8] (stars).

5.1. Production of a Long-Lived Isomeric State of the p-Isotope ^{181m}Ta

This role can be demonstrated by considering the example of data on the photodisintegration of tantalum isotopes. There are two tantalum isotopes in nature. These are stable ^{181}Ta (its abundance is 99.988%) and the long-lived isomer ^{180m}Ta ($E = 75.3$ keV, $T_{1/2} = 1.2 \times 10^{15}$ yr, $J^{\pi} = 9^{-}$, and the abundance is 0.012%). The ground state of the isotope ^{180g}Ta is short-lived ($E = 0.0$ keV, $T_{1/2} = 8.152$ h, and $J^{\pi} = 1^{+}$). Thus, ^{180}Ta is a unique nucleus—the only one natural isomer, ^{180m}Ta. Further, the natural production of the long-lived isotope ^{180m}Ta in s- and r-processes is prevented by the presence of the stable isotopes ^{179,180}Hf in nature (Fig. 7).

Since the cross sections for processes involving the production of the isotope ^{180}Ta in the ground and excited states are of great interest, several research groups performed experiments aimed at determining them by using various photon sources (radioactive isotopes, bremsstrahlung gamma radiation, and quasimonoenergetic photons from the annihilation process).

The results of those experiments differ substantially from one another in magnitude. For example, the amplitude of the cross section for the (γ, Sn) total photoneutron reaction,

$$\sigma(\gamma, Sn) = \sigma[(\gamma, 1n) + (\gamma, 2n) \qquad (4)$$
$$+ (\gamma, 3n) + \ldots]$$

(for medium-mass and heavy nuclei, it makes a dominant contribution to the full-photoabsorption cross
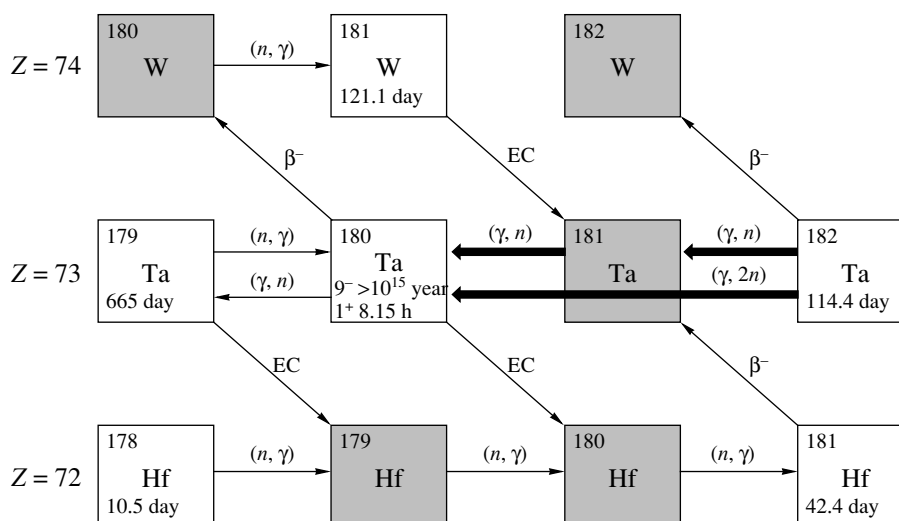
Fig. 7. ($N-Z$) diagram illustrating the possibilities for the production of the p-isotope ^{180m}Ta in (n, γ), $(\gamma, 1n)$, and $(\gamma, 2n)$ reactions: (gray squares) stable isotopes and (white squares) unstable isotopes (the lifetimes are indicated).

section), ranged from 280 to 420 mb in different experiments. The experimental cross sections also show some distinctions in shape, but, in all of them, there are two distinct maxima at an energy of 12 to 13 MeV and an energy of 15 to 16 MeV. Figure 8, which gives evaluated data from [24] along with their experimental counterparts obtained in [32, 33] for the ^{181}Ta nucleus with the aid of photons from annihilation processes, gives an example of the character of these discrepancies.

With the aim of experimentally testing the reliability of experimental and evaluated data that were obtained previously in a beam from the racetrack microtron of the Skobeltsyn Institute of Nuclear Physics at Moscow State University (electron accelerator of maximum energy 65 MeV), the relative yields of photoneutron reactions proceeding on a ^{181}Ta nucleus and leading to the emission of one to seven neutrons (Table 2) were measured with the aid of the gamma-activation method [34]. These new data are presented along with experimental data obtained earlier and reported in [32, 33]. Also presented in Table 2 are the results of respective calculations performed on the basis of the combined model (CM) of photonuclear reactions that was proposed in [27] and with the aid of the TALYS code [35], as well as data evaluated with the aid of the experimental−theoretical approach described above and formulated in [24].

It is noteworthy that the data obtained for $(\gamma, 1n)$ and $(\gamma, 2n)$ reactions with the aid of the gamma-activation method are at odds with the data obtained by the method of neutron-multiplicity sorting, but they agree with the evaluated data and with the results of CM and TALYS calculations. This is in-

dicative of the reliability of evaluations based on the proposed experimental−theoretical approach.

It should be emphasized that, in the gamma-activation experiment reported in [34], the contributions of the ground and isomeric states of the isotope ^{180}Ta could clearly be separated by using the lines of the corresponding gamma transitions in ^{180}W (103.6 keV) and ^{180}Hf (93.4 keV) nuclei produced in the β^- decay of the isotope ^{180g}Ta and electron capture in it.

This is in good agreement with the conclusions drawn in [36], where, in a beam of quasimonoenergetic photons from inverse Compton scattering, the authors measured and analyzed the cross section for the reaction ^{181}Ta$(\gamma, 1n)^{180}$Ta in the vicinity of the energy threshold of $Bn = 7.58$ MeV. They showed that this cross section, which, in accordance with Breit−Wigner theory in the presence of a single contribution of the neutron orbital angular momentum l, has the form

$$\sigma = \sigma_0 \left[\frac{E - Bn}{Bn} \right] p \qquad (5)$$

where $\sigma_0 = 207$ mb and $p = 0.96$ (this corresponds to $l + 1/2$), agrees with the presence of a specific mixture of s and p waves rather than a pure s wave. This indicates that the photodisintegration of the isotope ^{181}Ta proceeds via the emission of neutrons with orbital angular momenta of $l = 0$ and 1 both in the case of the transition to the ground state $[^{180g}$Ta$(1^+)]$ and in the case of the transition to the isomeric state $[^{180m}$Ta $(9^-)]$. Concurrently, those authors found that the cross section for the production of the isomeric state ^{180m}Ta is sensitive not only to the $E1$ strength
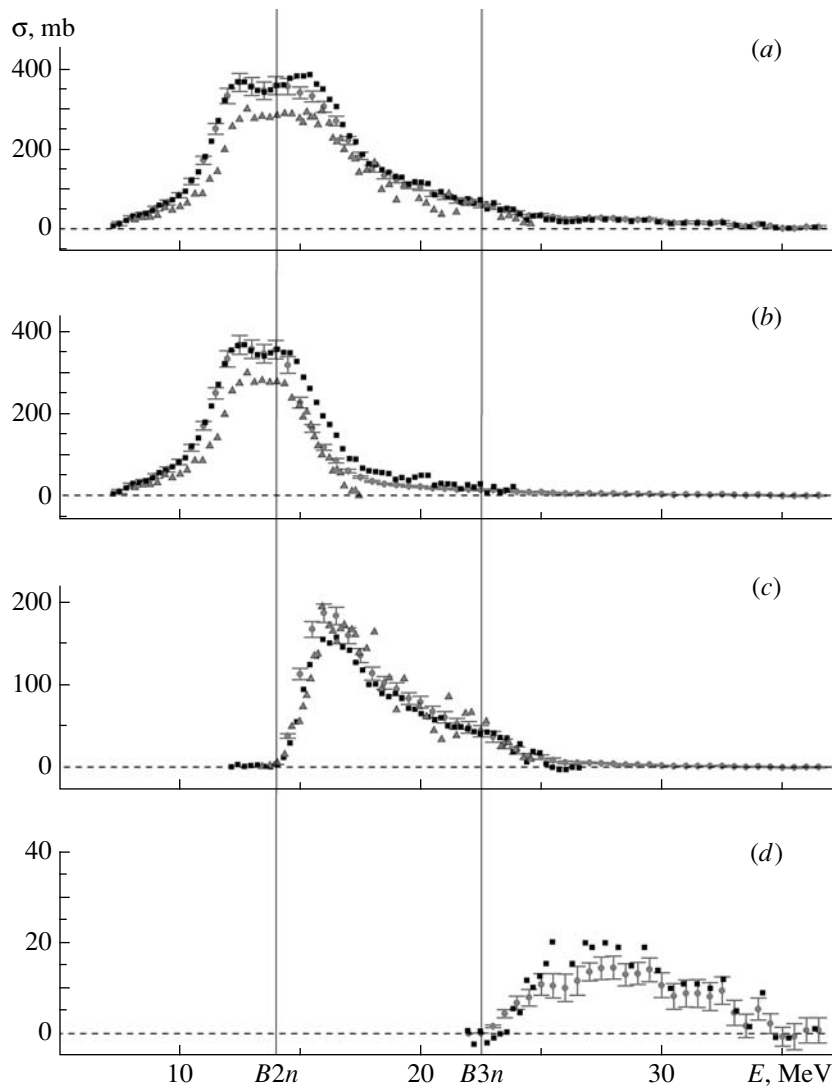
Fig. 8. Comparison for the ^{181}Ta nucleus of evaluated [24] (closed circles with error bars) and experimental reaction cross sections from (closed boxes) [32] and (closed triangles) [33]: (a) $\sigma(\gamma, Sn)$, (b) $\sigma(\gamma, 1n)$, (c) $\sigma(\gamma, 2n)$, and (d) $\sigma(\gamma, 3n)$.

function of the ^{181}Ta nucleus but also to the structure of ^{180}Ta nuclear levels from which cascade transitions to the isomeric ^{180m}Ta state proceed. In [37], the cross sections for the transitions to the ground state ^{180g}Ta and the isomeric state ^{180m}Ta were determined (see Table 3) by means of simultaneously detecting emitted neutrons (^{180g}Ta+^{180m}Ta) and x-ray lines at the energies of $E_{R\alpha1} = 55.79$ keV and $E_{R\alpha2} = 54.61$ keV (^{180m}Ta).

A rather large cross section (of up to several tens of millibarns) for the reaction ^{181}Ta$(\gamma, 1n)^{180m}$Ta, as well as the fact that the relative yields of the reactions ^{181}Ta$(\gamma, 1n)^{180g}$Ta and ^{181}Ta$(\gamma, 1n)^{180m}$Ta correspond to the concentrations (in percent) of the isotopes ^{181}Ta and ^{180m}Ta in their natural mixture (99.988% and 0.012%), gives sufficient grounds to

conclude that it is the reaction ^{181}Ta$(\gamma, 1n)^{180m}$Ta that underlies one of the dominant production mechanisms for the long-lived isomeric state ^{180m}Ta.

From the diagram in Fig. 7, it follows that there are two other processes that may lead to the production of the isotope ^{180m}Ta. These are neutrino capture by the ^{180}Hf nucleus ($\nu_e + {}^{180}$Hf $\rightarrow {}^{180m}$Ta $+ e^-$) and radiative neutron capture by the ^{179}Ta nucleus (^{179}Ta $+ n \rightarrow {}^{180m}$Ta $+ \gamma$). However, definitive conclusions on the contribution of these processes would be premature since the accuracy to which their cross sections are unknown is insufficient.

5.2. Production of the p-Isotope ^{196}Hg

Of equally great interest is the production of the bypassed p-isotope ^{196}Hg (its abundance is

Table 2. Relative yields of photonuclear reactions on the ^{181}Ta nucleus

Reaction	J^π	Reaction yield					
		Experiment			Evaluation	CM	TALYS
		[34]	[32]	[33]	[24]	[27]	[35]
^{181}Ta$(\gamma, 1n)^{180g}$Ta	1^+	0.99 ± 0.01	1	1	1	1	0.93
^{181}Ta$(\gamma, 1n)^{180m}$Ta	9^-	0.01 ± 0.01					0.07
^{181}Ta$(\gamma, 2n)^{179}$Ta	$7/2^-$	0.34 ± 0.07	0.24	0.42	0.37	0.29	0.32
^{181}Ta$(\gamma, 3n)^{178g}$Ta	1^+	$(1.80 \pm 0.40) \times 10^{-2}$	2.00×10^{-2}			2.4×10^{-2}	2.7×10^{-2}
^{181}Ta$(\gamma, 3n)^{178m}$Ta	7^-	$(5.00 \pm 1.00) \times 10^{-3}$					
^{181}Ta$(\gamma, 4n)^{177}$Ta	$7/2^+$	$(1.70 \pm 0.50) \times 10^{-2}$				1.0×10^{-2}	1.1×10^{-2}
^{181}Ta$(\gamma, 5n)^{176}$Ta	$(1)^-$	$(5.00 \pm 1.00) \times 10^{-3}$				3.7×10^{-3}	3.7×10^{-3}
^{181}Ta$(\gamma, 6n)^{175}$Ta	$7/2^+$	$(1.40 \pm 0.30) \times 10^{-3}$				1.2×10^{-2}	1.3×10^{-2}
^{181}Ta$(\gamma, 7n)^{175}$Ta	3^+					6.0×10^{-5}	6.0×10^{-5}
^{181}Ta$(\gamma, 1p)^{180g}$Hf	0^+					7.0×10^{-3}	8.0×10^{-4}
^{181}Ta$(\gamma, 1p)^{180m}$Hf	8^-	$(5.00 \pm 1.00) \times 10^{-4}$					3.0×10^{-5}
^{181}Ta$(\gamma, 1n1p)^{179g}$Hf	$9/2^+$					5.0×10^{-3}	1.0×10^{-3}
^{181}Ta$(\gamma, 1n1p)^{179m}$Hf	$25/2^-$	$(4.00 \pm 3.00) \times 10^{-5}$					

0.2%). Its production in s- and r-processes is blocked by the short-lived radioactive isotopes ^{197}Hg ($T_{1/2} = 64.1$ h) and ^{196}Au ($T_{1/2} = 6.2$ d). In [38], the photodisintegration of ^{196,197,198,199,200,201,204}Hg nuclei was studied in detail by the gamma-activation method. The experimental data obtained in this way

Table 3. Data from [37] on the cross sections for the reactions ^{181}Ta$(\gamma, 1n)^{180g}$Ta (σ^g) and ^{181}Ta$(\gamma, 1n)^{180m}$Ta (σ^m)

E, MeV	σ^{tot}, mb	σ^g, mb	σ^m, mb
9.2	48.0 (0.9)	45.0 (3.1)	3.0 (3.2)
9.7	73.0 (0.7)	66.0 (3.8)	6.0 (3.9)
10.5	109.0 (1.3)	103.0 (2.6)	6.0 (2.9)
10.9	143.0 (1.7)	130.0 (3.7)	13.0 (4.1)
11.5	234.0 (1.8)	219.0 (4.9)	15.0 (5.2)
12.3	383 (27)	329 (10)	54 (29)

were compared with the results of the calculations performed on the basis of the combined photonuclear-reaction model and with the aid of the TALYS code. It was found that the $(\gamma, 2n)$ cross section changes only slightly in response to changes in the mass number A. On the basis of data on the cross section for the reaction ^{198}Hg$(\gamma, 2n)^{196}$Hg, it was shown that the yield of the isotope ^{196}Hg is sufficiently large for the $(\gamma, 2n)$ photoneutron reaction in question to be its production mechanism in nature.

5.3. Reliability of Data on the Photodisintegration of Stable Osmium Isotopes and Production of the p-Isotope ^{184}Os

The situation around the photodisintegration of osmium isotopes is quite interesting from the point of view of the problems being discussed. In nature, there are seven stable osmium isotopes, ^{184,186,187,188,189,190,192}Os, their abundances being 0.02, 1.58, 1.60, 13.30, 16.10, 26.40, and 41%, respectively. The six isotopes that have the largest values of A can be produced in s- and r-processes, but the isotope ^{184}Os is a bypassed p-nucleus. It can

Fig. 9. Illustration of the position of the bypassed isotope ^{184}Os in the electron table of isotopes [39].

be produced (see Fig. 9) only in the photoneutron reactions ^{186}Os$(\gamma,\ 2n)^{184}$Os, ^{187}Os$(\gamma,\ 3n)^{184}$Os, ^{188}Os$(\gamma, 4n)^{184}$Os, ...

To date, only the cross section for the reaction ^{186}Os$(\gamma, 2n)^{184}$Os have been determined from the required experimental data. It was obtained in a beam of quasimonoenergetic protons from annihilation processes by using the method of neutron-multiplicity sorting [40].

In Fig. 10, the experimental cross sections for the reactions ^{186}Os$(\gamma, 1n)^{185}$Os and ^{186}Os$(\gamma, 2n)^{184}$Os are contrasted against the cross sections evaluated within the approach outlined above, as well as against the functions $F_{1,2}$ obtained on the basis of experimental and theoretical data. One can clearly see that the reliability of the experimental data being considered is questionable, since, at energies in the region of $E > 18$ MeV, the function F_2^{expt} lies in the region of values in excess of the physically reasonable limit of 0.50, while the function F_1^{expt} takes negative values forbidden physically.

The data in Fig. 10 show how the data on the cross sections for the reactions ^{186}Os$(\gamma, 1n)^{185}$Os and ^{186}Os$(\gamma, 2n)^{184}$Os are corrected within the proposed experimental–theoretical approach to their evaluation.

In [40], the $(\gamma, 1n)$, $(\gamma, 2n)$, and $(\gamma, 3n)$ cross sections were measured for the remaining stable isotopes ^{188,189,190,192}Os. All cross sections for the respective reactions on isotopes that can be produced in s- and r-processes and on the isotope that can be produced only in the p-process prove to be close both in magnitude and shape and in the energy position. This is illustrated by Fig. 11, in which the results of the calculations that rely on the combined photonuclear-reaction model and which describe well experimental data are presented. Therefore, there are reasons to state that the reaction ^{186}Os$(\gamma, 2n)^{184}$Os may be the production mechanism for the bypassed p-isotope ^{184}Os.

5.4. Photoneutron Reactions near the Threshold in s- and r-Processes

In connection with the growth of interest in problems of the formation of chemical elements, data on the photodisintegration of nuclei at energies in the vicinity of the nucleon threshold proved to be in great demand in recent years [41–44]. This interest is motivated by the circumstance that the aforementioned r-process is operative primarily in the region of neutron-rich nuclides, where radiative neutron capture by unstable nuclei have not yet received adequate study. Within the Hauser–Feshbach model, the statistical
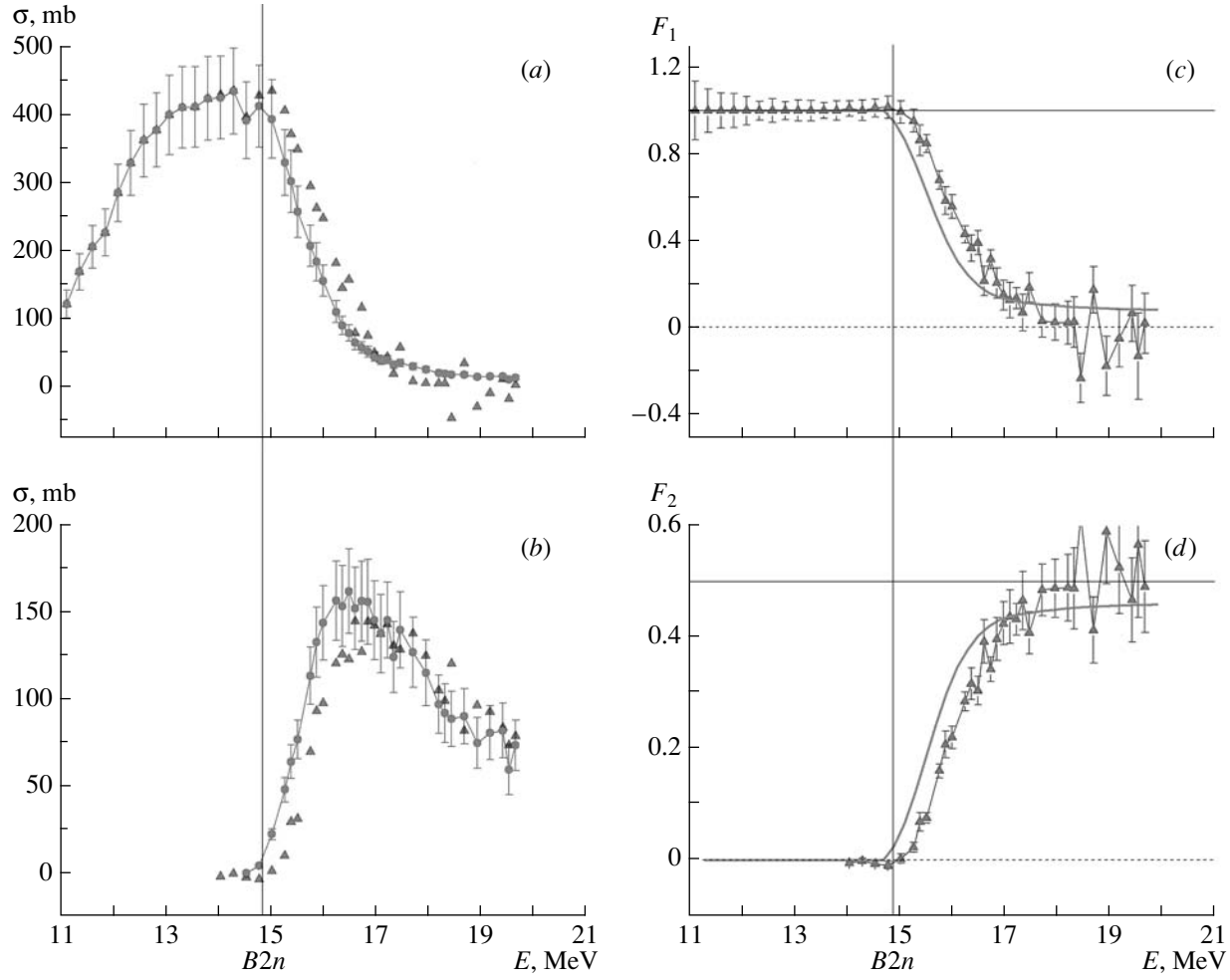
Fig. 10. Energy dependence of the (closed circles) experimental and (closed triangles) evaluated [39] cross sections for the reactions (a) ^{186}Os$(\gamma, 1n)^{185}$Os and (b) ^{186}Os$(\gamma, 2n)^{184}$Os, as well as of the functions (c) F_1^{expt} and (d) F_2^{expt} obtained on the basis of experimental data and the results of theoretical calculations [27, 28] (curves).

cross section for radiative neutron capture is formulated in terms of neutron- and photon-transfer coefficients (T_n and T_γ, respectively). In the formation of a state at an excitation energy E upon neutron capture, the coefficient $T_n(E)$ is determined by the neutron optical potential. In the the gamma-decay channel, $T_\gamma(E)$ is the photon-transfer coefficient summed over all first-chance decays. Thus, the total coefficient can be represented in the form

$$T_\gamma(E) = \int_m T_\gamma^m(E_\gamma)\rho(E_m)dE_m, \qquad (6)$$

where $\rho(E_m)$ is the level density for participant states; $E_\gamma = E - E_m$; and the partial coefficient

$$T_\gamma^m(E_\gamma) = 2\pi E_\gamma^3 f(E_\gamma)\!\downarrow \qquad (7)$$

is determined by the strength function $f(E_\gamma)\!\downarrow$, which, according to the Brink hypothesis, can be

obtained in studying the photodisintegration of the nucleus being considered,

$$f(E_\gamma)\!\downarrow \approx f(E_\gamma)\!\uparrow. \qquad (8)$$

The strength function $f(E_\gamma)\!\uparrow$ is related to the photoabsorption cross section by the equation

$$\sigma_{\text{abs}}(E_\gamma) = 3(\pi\hbar c)^2 E_\gamma f(E_\gamma)\!\uparrow. \qquad (9)$$

In turn, the latter is related to the photoneutron cross section by the equation

$$\sigma_{\gamma,n}(E_\gamma) = \sigma_{\text{abs}}(E_\gamma)T_n/(T_n + T_\gamma). \qquad (10)$$

Thus, the low-energy region (extending to the energy of the first excited state—1 MeV in the majority of heavy nuclei) of the giant dipole resonance (GDR) has a direct bearing on the cross section for radiative neutron capture. In the vicinity of the nucleon threshold, M1 and pygmy resonances (dipole vibrations of the neutron excess in the nucleus about
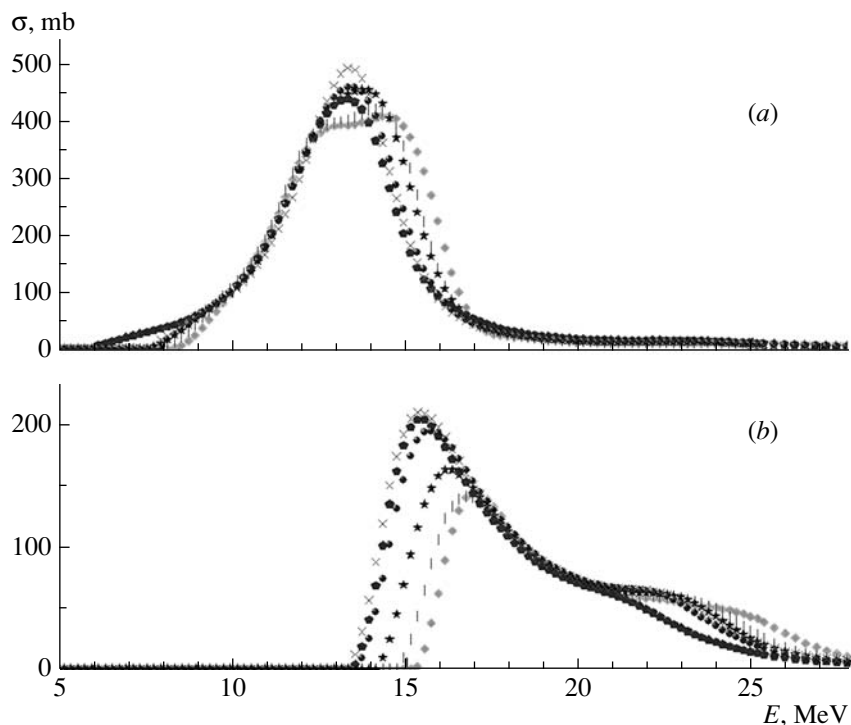
Fig. 11. Cross sections calculated within the combined photonuclear-reaction model [27, 28] for the (a) (γ, n) and (b) $(\gamma, 2n)$ reactions on the stable osmium isotopes: (closed diamonds) ^{184}Os, (vertical bars) ^{186}Os, (stars) ^{188}Os, (pentagons) ^{189}Os, (closed circles) ^{190}Os, and (inclined crosses) ^{192}Os.

its $N = Z$ core) are observed in addition to the giant E1 resonance. Although the intensities of these excitations are weaker than the GDR intensity, the gamma decays of a compound state to the ground state of the nucleus through pygmy E1 and M1 resonances make a sizable contribution to radiative neutron capture. Therefore, a correct representation of the photon strength function in terms of the low-energy GDR region and, additionally, strengths of pygmy E1 and M1 resonances may serve as a tool for predicting the radiative-capture cross section within the statistical model. This renders the role of photoneutron reactions in astrophysical processes still more important and the problem of obtaining data on cross sections for photoneutron reactions—first of all, $(\gamma, 1n)$ reactions—still more pressing.

6. CONCLUSIONS

Although experimental data on the photodisintegration of nuclei were predominantly obtained with statistical errors of about 10%, there are systematic discrepancies of 60 to 100% between the results of different experiments aimed at determining cross sections for partial reactions. From the point of view of the application of photonuclear data in solving astrophysics problems, it is also worth noting that there is

a want of many data necessary for this. In this connection, new investigations, both experimental and theoretical, in the realms of photonuclear reactions, as well as the development of evaluation methods that could contribute to removing systematic uncertainties in data and substantially improving the reliability of deduced information, are of crucial importance.

The results obtained by studying photonuclear reactions indicate that atomic nuclei contain huge energy, which may serve as the energy of stars, in which new nuclei that were absent at early stages of the development of the Universe arise. Not only the development of astronomical methods of investigations and methods based on the use of space vehicles, but also the refinement of nuclear-physics methods contributes to studying the properties of the Universe. To a great extent, a further development of nuclear-astrophysics methods and the improvement of their accuracy are stimulated by the recent discoveries, such as discovery of dark matter and dark energy and of the inflation of the Universe.

REFERENCES

1. E. M. Burbidge, G. R. Burbidge, W. A. Fowler, and F. Hoyle, Rev. Mod. Phys. **29**, 547 (1957).

2. B. S. Ishkhanov, I. M. Kapitonov, and N. P. Yudin, *Particles and Nuclei* (Mosk. Gos. Univ., Moscow, 2005) [in Russian].

3. V. Arnold and S. Goriely, Phys. Rep. **384**, 1 (2003).

4. E. Anders and N. Grevesse, Geochim. Cosmochim. Acta **53**, 197 (1989).

5. H. Palme, H. Beer, and H. H. Vogt, in *Landoldt-Börnstein, New Series, Group VI, Astronomy and Astrophysics* (Springer, Berlin, 1993), Subvol. 3a, p. 15.

6. B. S. Ishkhanov and I. M. Kapitonov, *Interaction of Electromagnetic Radiation with Nuclei* (Mosk. Gos. Univ., Moscow, 1979) [in Russian].

7. B. L. Berman and S. C. Fultz, Rev. Mod. Phys. **47**, 713 (1975).

8. H. Utsunomiya, H. Goriely, S. Kamata, et al., Phys. Rev. C **84**, 055805 (2011).

9. S. S. Dietrich and B. L. Berman, At. Data Nucl. Data Tables **38**, 199 (1988).

10. A. V. Varlamov, V. V. Varlamov, D. S. Rudenko, and M. E. Stepanov, INDC(NDS)-394, IAEA NDS (Vienna, Austria, 1999).

11. Russia Lomonosov Moscow State University Skobeltsyn Institute of Nuclear Physics Centre for Photonuclear Experiments Data, Nuclear Reaction Database (EXFOR). http://cdfe.sinp.msu.ru/exfor/index.php; USA National Nuclear Data Center, CSISRS and EXFOR Nuclear Reaction Experimental Data, Database.http://www.nndc.bnl.gov/exfor/exfor00.htm

12. B. S. Ishkhanov, I. M. Kapitonov, E. V. Lazutin, et al., Sov. J. Nucl. Phys. **12**, 484 (1971).

13. A. Veyssière, H. Beil, R. Bergère, et al., Nucl. Phys. A **227**, 513 (1974).

14. R. L. Bramblett, J. T. Caldwell, R. R. Harvey, and S. C. Fultz, Phys. Rev. **133**, B 869 (1964); J. T. Caldwell, R. L. Bramblett, B. L. Berman, et al., Phys. Rev. Lett. **15**, 976 (1965).

15. V. V. Varlamov, B. S. Ishkhanov, D. S. Rudenko, and M. E. Stepanov, Phys. At. Nucl. **67**, 2107 (2004).

16. V. V. Varlamov, B. S. Ishkhanov, M. E. Stepanov, and D. S. Rudenko, Bull. Russ. Acad. Sci.: Phys. **7**, 1733 (2003).

17. B. L. Berman, R. E. Pywell, S. S. Dietrich, et al., Phys. Rev. C **36**, 1286 (1987).

18. V. V. Varlamov and B. S. Ishkhanov, INDC(CCP)-433, IAEA NDS (Vienna, Austria, 2002).

19. V. V. Varlamov, N. G. Efimkin, B. S. Ishkhanov, and V. V. Sapunenko, Vopr. At. Nauki Tekh., Ser.: Yad. Konst., No. 1, 52 (1993).

20. V. V. Varlamov, N. N. Peskov, D. S. Rudenko, and M. E. Stepanov, Vopr. At. Nauki Tekh., Ser.: Yad. Konst., Nos. 1−2, 48 (2003).

21. V. V. Varlamov, B. S. Ishkhanov, V. N. Orlin, and V. A. Chetvertkova, Bull. Russ. Acad. Sci.: Phys. **74**, 833 (2010).

22. V. V. Varlamov, B. S. Ishkhanov, V. N. Orlin, and S. Yu. Troshchiev, Bull. Russ. Acad. Sci.: Phys. **74**, 842 (2010).

23. V. V. Varlamov, B. S. Ishkhanov, and V. N. Orlin, Phys. At. Nucl. **75**, 1339 (2012).

24. B. S. Ishkhanov, V. N. Orlin, N. N. Peskov, M. E. Stepanov, and V. V. Varlamov, Preprint No. 2013-1/884, NIIYad. Fiz. MGU (Inst. Yad. Fiz., Mosk. Gos. Univ., Moscow, 2013).

25. B. S. Ishkhanov, V. N. Orlin, and S. Yu. Troshchiev, Phys. At. Nucl. **75**, 353 (2012).

26. B. L. Berman, J. T. Caldwell, R. R. Harvey, et al., Phys. Rev. **162**, 1098 (1967).

27. B. S. Ishkhanov and V. N. Orlin, Phys. Part. Nucl. **38**, 232 (2007).

28. B. S. Ishkhanov and V. N. Orlin, Phys. At. Nucl. **71**, 493 (2008).

29. V. V. Varlamov, B. S. Ishkhanov, V. N. Orlin, N. N. Peskov, and M. E. Stepanov, Phys. At. Nucl. **76**, 1403 (2013).

30. A. Leprètre, H. Beil, R. Bergère, et al., Nucl. Phys. A **219**, 39 (1974).

31. S. C. Fultz, B. L. Berman, J. T. Caldwell, et al., Phys. Rev. **186**, 1255 (1969).

32. R. Bergère, H. Beil, and A. Veyssière, Nucl. Phys. A **121**, 463 (1968).

33. R. L. Bramblett, J. T. Caldwell, G. F. Auchampaugh, and S. C. Fultz, Phys. Rev. **129**, 2723 (1963).

34. B. S. Ishkhanov and S. Yu. Troshchiev, Moscow Univ. Phys. Bull. **66**, 219 (2011).

35. S. Agostinelli et al., Nucl. Instrum. Methods Phys. Res. A **506**, 250 (2003).

36. H. Utsunomiya, H. Akimune, S. Goko, et al., Phys. Rev. C **67**, 015807 (2003).

37. S. Goko, H. Utsunomiya, S. Goriely, et al., Phys. Rev. Lett. **96**, 192501 (2006).

38. B. S. Ishkhanov, V. N. Orlin, and S. Yu. Troshchiev, Phys. At. Nucl. **74**, 706 (2011).

39. Russia Lomonosov Moscow State University Skobeltsyn Institute of Nuclear Physics Centre for Photonuclear Experiments Data, Digital Map of Atomic Nuclei. http://cdfe.sinp.msu.ru/services/ground/index.html

40. B. L. Berman, D. D. Faul, R. A. Alvarez, et al., Phys. Rev. C **19**, 1205 (1979).

41. H. Utsunomiya, S. Goriely, M. Kamata, et al., Phys. Rev. C **80**, 055806 (2009).

42. H. Utsunomiya, S. Goriely, H. Akimune, et al., Phys. Rev. C **81**, 035801 (2010).

43. H. Utsunomiya, S. Goriely, H. Akimune, et al., Phys. Rev. C **82**, 064610 (2010).

44. T. Kondo, H. Utsunomiya, S. Goriely, et al., Phys. Rev. C **86**, 014316 (2012).